Journal of the Korean Nuclear Society
Volume 22, Number 2, June 1990

Measurements of X-Ray Production Cross-Sections for 0.5~1.2-MeV Proton Beam

Hae-iLL BAK and Jun-Gyo BAK
Department of Nuclear Engineering, Seoul National University

(Received November 15, 1989)

0.5~1.2-MeV 양성자빔에 대한 X-선 발생단면적의 측정

박혜일 · 박준교
서울대학교 원자핵공학과

(1989. 11. 15 접수)

Abstract

The measurements of X-ray production cross-sections for 0.5~1.2-MeV proton beam are carried out on Cu and Au. For this experiment, the proton beam generated from the SNU 1.5-MV Tandem Van de Graaff accelerator is incident on the target. The X-rays and the backscattered protons from the irradiated target are detected simultaneously by the Si(Li) X-ray detector and the SSB (Silicone Surface Barrier) charged particle detector. The measured values of X-ray production cross-sections are compared with other experimental values and theoretical values such as the PWBA (Plane Wave Born Approximation) and the ECPSSR (Perturbed Stationary State corrected Energy loss, Coulomb deflection, Relativistic effects) values. For measured cross-sections near 1.0-MeV proton energy, the ECPSSR (D.D. Cohen et al., 1985) shows better agreement than the PWBA. Particularly, that of Au for 1.2-MeV proton beam is 9.69±0.39 barns which deviates from the ECPSSR by less than 5%, and the experimental data for 0.5~1.2-MeV proton agree with most of other experimental values within 30%.

요 약

0.5~1.2-MeV 양성자빔에 대한 X-선 발생단면적의 측정을 Cu와 Au에 대해 수행하였다. 이 실험에서는 SNU 1.5-MV 탄뎀 반데그라프 가속기에서 얻은 양성자빔을 표적에 입사시켰다. 여기서 방출된 X-선과 후방산란된 양성자는 Si(Li) X-선 검출기와 SSB(Silicone Surface Barrier) 하전입자 검출기를 이용해 동시 측정하였다. 그리하여 측정된 X-선 발생단면적은 다른 실험치들 및 PWBA (Plane Wave Born Approximation)와 ECPSSR(Perturbed Stationary State corrected Energy loss, Coulomb deflection, Relativistic effects)인 이론치들과 비교하였다. 1.0-MeV 근처의 양성자에너지에 대해 측정치는 PWBA 값보다는 ECPSSR(D.D. Cohen et al., 1985) 값에 더 잘 일치함을 보였다.

특히, Au의 측정치는 1.2-MeV 양성자빔에 대해 9.69±0.39 barns이었고, ECPSSR 이론치와는 5% 이내로 일치했으며, 0.5~1.2-MeV 양성자에 대한 실험치는 대부분의 다른 실험치들과 30% 이내로 일치했다.

I. Introduction

The study of X-ray was initiated with the discovery of X-ray produced from the bombardment of electrons on the Pt-Ba Target in the cathode-ray tube (W.C. Roentgen, 1895). In 1913, W.H. Bragg discovered that the radiation of the continuous spectrum, on which the charateristic X-ray of the anode material is superimposed, is emitted from the X-ray tube. J. Chadwich (1912, 1913), A.S. Russel and J. Chadwick (1914), and J.J. Thomson (1914) performed the first ion-atom collision experiments by bombarding various materials with energetic alpha particles from radioactive sources, and explained the process of inner-shell ionization from the emission of the characteristic X-rays. Thereafter a unified picture of theories for the ionization process was realized by P. Auger (1925, 1926), C.L. Kronig and R.de L. Coster(1935). Thus it was possible to calculate the inner-shell ionization cross-sections theoretically by introducing several approximations. The important approximation methods were the PWBA (Plane Wave Born Approximation) and the ECPSSR (Perturbed Stationary State corrected Energy loss, Coulomb deflection, Relativistic effects) methods as quantum mechanical approach and BEA (Binary Encounter Approximation) and SCA (Semi-Classical Approximation) methods as classic mechanical approach. And these inner-shell ionization cross-sections can be related to the experimental X-ray production cross-sections from the X-ray spectroscopic data given by W. Bambynek and J.H. *Scofield.*

Recently the applied field of X-rays on non destructive analysis has been activated according to the development of the high resolution X-ray spectrometers. Among these non-destructive analysis methods, PIXE (Proton Induced X-ray Emission) method has been highlighted in various *fields of biology, archaeology and geology, etc.* Therefore, further evaluation of the proton-induced X-ray production cross-sections is considered to be essential task to improve the usefulness of the PIXE analysis.

The present paper reports on the measurements of X-ray production cross-sections for Cu and Au. This experiment was carried out for 0.5~1.2-MeV proton beam generated from the SNU 1.5-MV Tandem Van de Graaff accelerator. The beam energy was determined by using the energy calibration formula deduced from F^{19} $(p,\alpha\gamma)O^{16}$ nuclear resonance reaction experiment (1). The X-ray production cross-sections were measured by simultaneous detection of the backscattered protons and the X-rays from the target irradiated by proton beam. And these values were compared with other experimental values as well as the theoretical values (PWBA and ECPSSR values) with the view of being utilized as for the basic data of PIXE analysis.

II. Experimental Method

The SNU 1.5-MV Tandem Van de Graaff accelerator was used to produce proton beam ranging from 0.5 to 1.2 MeV. The beam energy was determined by the calibration formula for the proton beam energy versus the analysing-magnet current deduced from F^{19} $(p,\alpha\gamma)$ O^{16} nuclear resonance reaction experiment (1).

In the measurements of X-ray production cross-

sections, the energy loss of the proton beam in the target should be taken into account because X-ray production cross-sections depend on the beam energy. These energy loss effects were limited to the value of 1 % in order to measure cross-sections of Cu and Au for the incident energy. For this purpose, the 70 $\mu g/cm^2$ -Cu and the 42 $\mu g/cm^2$ -Au samples were prepared. These samples were deposited on the 6 μm and the 3.5 μm mylar film backings, respectively. The target chamber was constructed as shown in Fig. 1 for simultaneous detection of the X-rays and the backscattered protons from the irradiated target. It contained a 9.5 mmϕ carbon collimator to define the beam size and a 4 mmϕ brass collimator to reduce the measurement errors which arise from the non-uniformity of the beam current density. The proton beam was incident on the target for normal incidence.

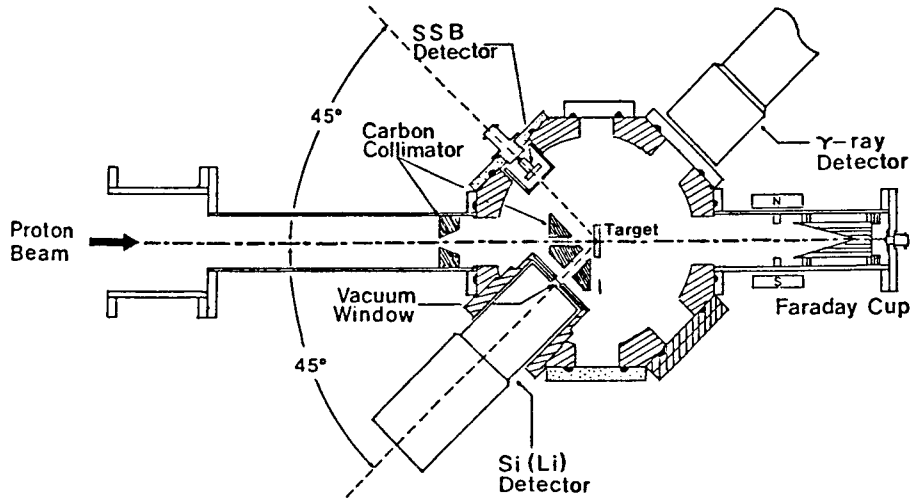

Fig. 1. Target Chamber for Simultaneous PIXE and RBS Analysis.

The characteristic X-rays and the backscattered protons were detected simultaneously by the Si(Li) detector with a resolution of 175 eV FWHM at 5.9 keV Mn K_α line from Fe-55 and the SSB detector with a 17 keV resolution for 5.49 MeV alpha from Am-241.

These two detectors were located at 45° to the incident beam line. This simultaneous detection of the backscattered protons and the X-rays from the target can effectively eliminate error effects which result from both the target thickness and the intensity of the incident proton beam. The solid angles of the Si(Li) detector and the SSB detector were 14.75 mstr. and 0.3831 mstr., respectively.

Elements(Z)	Transition	Energy (keV)	ε_w	ε_{air}	ε_D
Cu(29)	K_α	8.041	0.992	0.992	1.00
	K_β	8.907	0.995	0.994	1.00
Au(79)	L_ι	8.494	0.994	0.992	1.00
	L_α	9.704	0.996	0.995	1.00
	L_β	11.443	0.997	0.997	1.00
	L_γ	13.381	0.998	0.998	1.00

Table 1. X-ray Transmission and Detection Efficiency.

The intrinsic efficiency of the Si(Li) detector was determined by using the data of the Canberra catalogue (ε_D), and the attenuation factors(ε_W, ε_{air}) of the X-rays for the 22 μm polypropylene vacuum window and a 7.27 mm air layer were calculated from the available data (2, 3). These values are shown in Table 1. The beam currents were varied between 1 and 10 nA.

III. Analysis of Data and Error

A. Data analysis

The typical energy spectra of the K and L X-rays produced from Cu and Au by the proton impact are shown in Fig.2 and Fig.3 with the backscattered proton spectra.

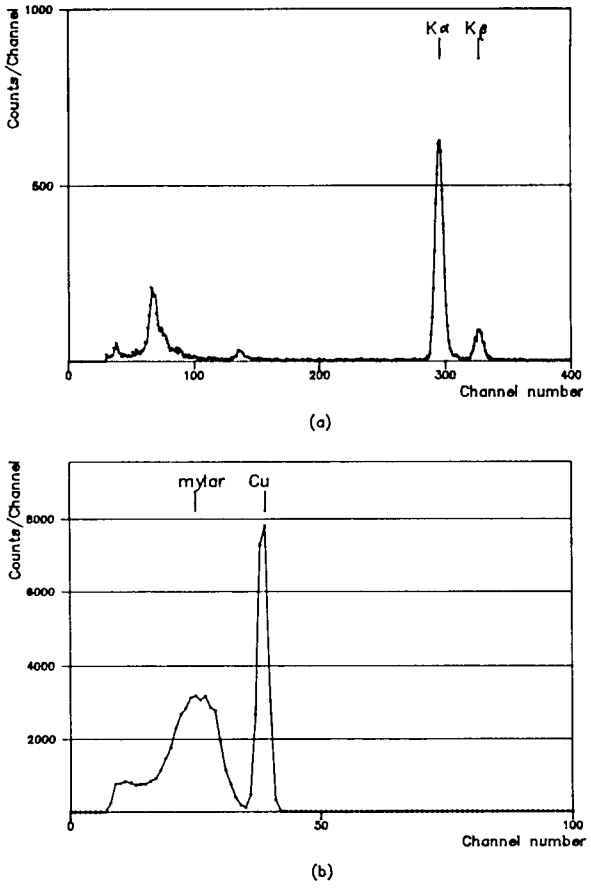

Fig. 2. X-ray and RBS Spectra from 69 μg/cm^2 -Cu Target for 0.5169 MeV Proton Beam ; (a) X-ray Spectrum (0.028 keV/Ch.), (b) RBS Spectrum (12.48 keV/Ch.).

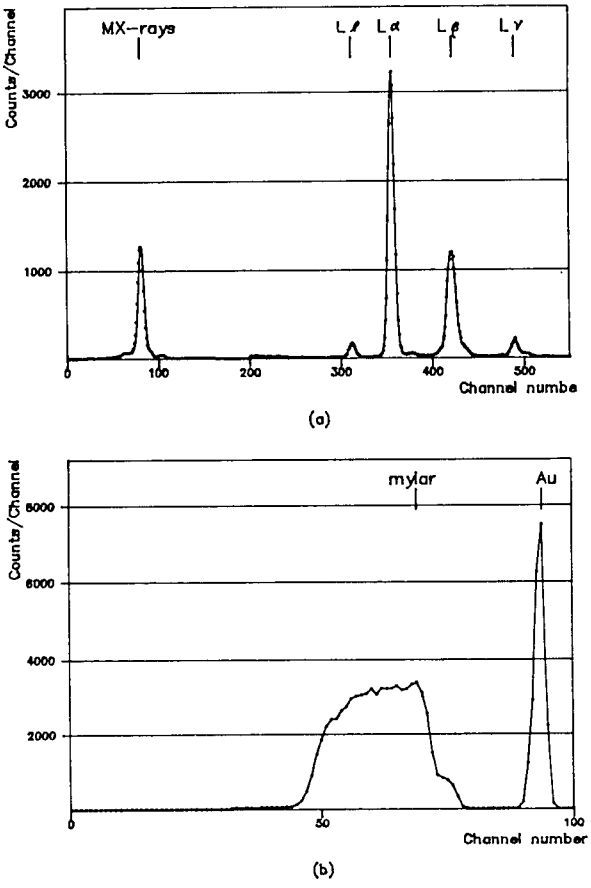

Fig. 3. X-ray and RBS Spectra from 42 μg/cm^2 –Au Target for 1.202 MeV Proton Beam ; (a) X-ray Spectrum (0.028 keV/Ch.), (b) RBS Spectrum (12.48 keV/Ch.).

Assuming that the L-shell X-ray production is isotropic, the X-ray production cross-section σ_x, is obtained from

$$\sigma_x(E) = 4\pi \frac{I_x \Omega_p \varepsilon_p}{I_p \Omega_x \varepsilon_x} \left(\frac{d\sigma_R}{d\Omega}\right), \quad (1)$$

where Ω_p and Ω_x are the solid angles subtended by the SSB detector and the Si(Li) detector, respectively. I_p and I_x are the peak areas for the backscattered protons and the X-rays, respectively. The latter was obtained by assuming that the corresponding peaks follow the Gaussian distribution, and taking account of the branching ratio for the characteristic X-rays (4~7). ε_p and ε_x are the detection efficiencies ($\varepsilon_x = \varepsilon_D \times \varepsilon_W \times \varepsilon_{air}$, Table 1). $\left(\frac{d\sigma_R}{d\Omega}\right)$ is the Rutherford scattering cross-section given by

$$\left(\frac{d\sigma_R}{d\Omega}\right) = \left(\frac{Z_1 Z_2 e^2}{4E}\right)^2 \frac{4}{\sin^4\theta} \frac{\left[\left\{1-\left(\frac{M_1}{M_2}\sin\theta\right)^2\right\}^{\frac{1}{2}} + \cos\theta\right]^2}{\left\{1-\left(\frac{M_1}{M_2}\sin\theta\right)^2\right\}^{\frac{1}{2}}},$$

where E is the incident beam energy in MeV, θ is the scattering angle of beam. Z_1 and M_1 are the charge and the mass of the projectile, Z_2 and M_2 the charge and the mass of the target.

B. Error Analysis

In the present experiment, an error analysis has been carried out using the following error propagation formula for Eq.(1),

$$\left(\frac{\delta\sigma_x}{\sigma_x}\right)^2 = \left[\left(\frac{\delta I_x}{I_x}\right)^2 + \left(\frac{\delta\varepsilon_p}{\varepsilon_p}\right)^2 + \left(\frac{\delta I_p}{I_p}\right)^2 + \left(\frac{\delta\varepsilon_x}{\varepsilon_x}\right)^2\right]. \quad (2)$$

In Eq. (2), the statistical errors, $\left(\frac{\delta I_x}{I_x}\right)$ and $\left(\frac{\delta I_p}{I_p}\right)$ were the main contributors to the results. And other terms were neglected because the relative errors were below 1%. The peak area, I_{pA}, is the value obtained by subtracting the area due to the background, I_b, from the total peak area, I_t. And the error of the peak area, δI_{pA}, is

$$\delta I_{pA} = \sqrt{(\delta I_t)^2 + (\delta I_b)^2} = \sqrt{I_t + I_b}.$$

As the ratio of I_b to I_t is less than 0.01, I_b can be neglected. Thus the above Eq.(2) can be rewritten as

$$\left(\frac{\delta\sigma_x}{\sigma_x}\right) = \left(\frac{1}{I_x} + \frac{1}{I_p}\right)^{\frac{1}{2}}$$

IV. Results

The experimental X-ray production cross-sections can be compared with the theoretical subshell-ionization cross-sections (PWBA, ECPSSR) by using the subshell fluorescence yields, Coster-Kronig(CK) transition probabilities and the fractions of the radiative transitions in each subshell group(8,9).

In the K-shell case, the relation between the theoretical ionization cross-section, σ_K, and the X-ray production cross-section, σ_K^X, is given by

$$\sigma_K^X = \omega_K \sigma_K,$$

where ω_K is the fluorescence yield calculated from the semi-empirical formula (8),

$$[\omega_k/(1-\omega_k)]^{\frac{1}{4}} = 0.015 + 0.0327Z - 0.64\times10^{-4}Z^2.$$

The partial and total L X-ray production cross-sections, $\sigma_{L_\gamma}^X$, σ_L^X, ($\gamma = \alpha, \beta, \gamma, \ell$) are related to the subshell-ionization cross-sections, $\sigma_{L_n}^X$, (n = 1, 2, 3) by the formula,

$$\sigma_\ell^X = \{\sigma_{L1}(f_{13}+f_{12}f_{23}) + \sigma_{L2}f_{23} + \sigma_{L3}\}\omega_3 F_{3\ell}$$

$$\sigma_{L_\alpha}^X = \{\sigma_{L1}(f_{13}+f_{12}f_{23}) + \sigma_{L2}f_{23} + \sigma_{L3}\}\omega_3 F_{3\alpha}$$

$$\sigma_{L_\beta}^X = \sigma_{L1}\omega_1 F_{1\beta} + (\sigma_{L1}f_{12} + \sigma_{L2})\omega_2 F_{2\beta} + \{\sigma_{L1}(f_{13}+f_{12}f_{23}) + \sigma_{L2}f_{23} + \sigma_{L3}\}\omega_3 F_{3\beta}$$

$$\sigma_{L_\gamma}^X = \sigma_{L1}\omega_1 F_{1\gamma} + (\sigma_{L1}f_{13} + \sigma_{L2})\omega_2 F_{2\gamma}$$

$$\sigma_{Lx}^X = \sigma_{L\ell}^X + \sigma_{L\alpha}^X + \sigma_{L\beta}^X + \sigma_{L\gamma}^X.$$

Table 2. Fluorescence Yields, Coster-Kronig Transition Probabilities, Radiative Decay Rates of Au.

Parameters	Theoretical values
ω_1	0.105
ω_2	0.357
ω_3	0.327
f_{12}	0.083
f_{13}	0.644
f_{23}	0.132
$F_{1\beta}$	0.747
$F_{1\gamma}$	0.225
$F_{2\beta}$	0.799
$F_{2\gamma}$	0.179
$F_{3\alpha}$	0.787
$F_{3\beta}$	0.172
$F_{3\gamma}$	0.040

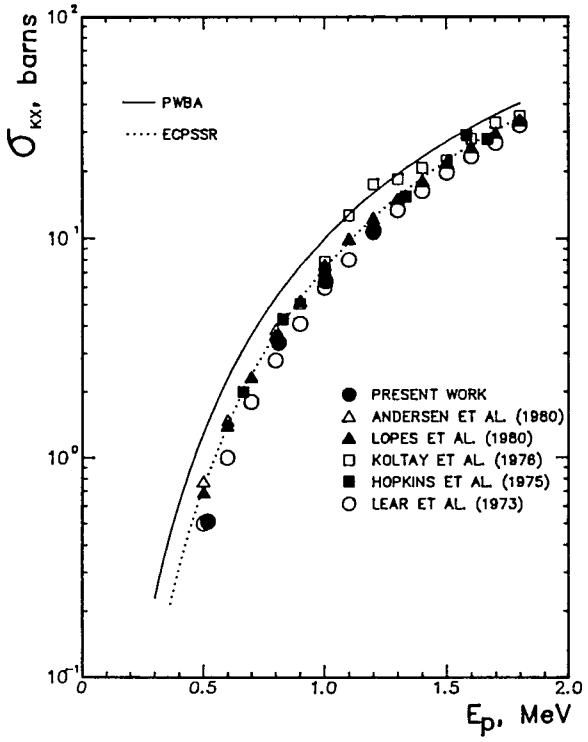

Fig. 4. Total K-shell X-ray Production Cross-Section for Cu vs. Proton Energy.

where ω_i is the i-th subshell fluorescence yield, f_{ij} is the CK transition yield linking the subshell i and j ($i \neq j$; i=1, 2, 3 j=1, 2, 3), and $F_{i\gamma}$ is the fraction of the radiation width of the subshell L_i contained in the y-th spectral line (8). These parameters for Au are given in Table 2.

The results of the K and L X-ray production cross-sections of Cu and Au are shown in Fig.4 and Fig.5, and are listed in Table 3 for the proton beam energies ranging from 0.5 to 1.2 MeV. The PWBA and ECPSSR values were given by O. Benka, G. Basbas and D.D. Cohen(10~12).

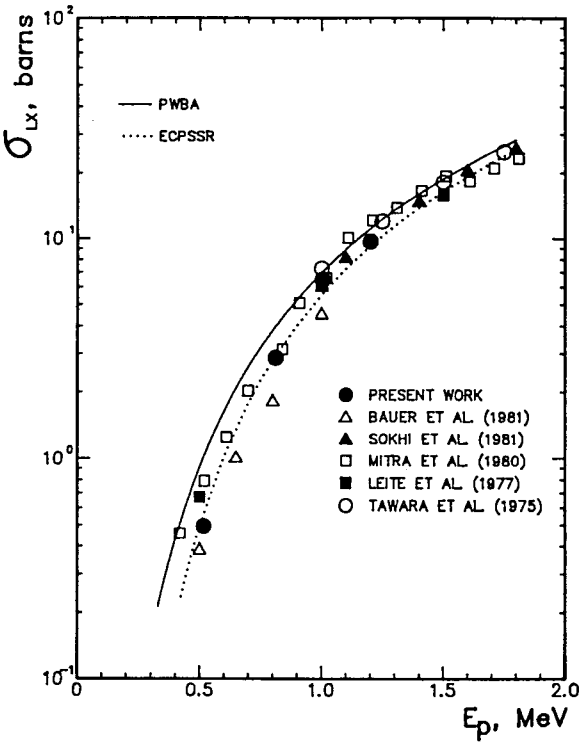

Fig. 5. Total L-shell X-ray Production Cross-Section for Au vs. Proton Energy.

The statistical errors of the measured values shown in Table 3 are in the range of 3~8%. The measured cross-section values for Cu and Au plotted in Fig.4 and Fig.5 show fairly good agreement with other experimental data (7,13~21), but the comparison for 0.5 MeV energy presents certain

degree of discrepancy and suggests further evaluations for low energy cross-section data. Particularly, the present measurements agree with the

Table 3. Comparisons of the Theoretical Values with the Present Work for K and L X-ray Production Cross-Sections of Cu and Au, Respectively in Barns.

Elements	Proton beam energy (MeV)	Present work	Theoretical values	
			PWBA	ECPSSR
Cu	0.5169	0.510±0.024	1.43	0.858
	0.813	3.35 ±0.06	5.63	3.92
	1.003	6.40 ±0.18	10.1	7.42
	1.202	10.8 ±0.8	16.0	12.4
Au	0.5169	0.494±0.039	1.01	0.583
	0.813	2.87 ±0.15	3.99	2.95
	1.003	6.87 ±0.28	7.04	5.57
	1.202	9.69 ±0.39	11.1	9.23

values of R. Lear et al.(13) and S.K. Mitra et al.(18) within 5% deviation for 1.0-MeV proton beam. Compared with theoretical values near 1.0-MeV proton energy, the ECPSSR (D.D. Cohen et al., 1985) indicates better agreement than the PWBA as shown in Table 3. Particularly, the value of Au for 1.2 MeV proton agrees with the ECPSSR within 5%. Also, Fig.4 and Fig.5 show that the trend of the variation of measured cross-sections is very similar to that of the ECPSSR and PWBA curves.

V. Conclusion

As mentioned above, the results show that the measured values of Cu and Au for 0.5~1.2-MeV proton beam agree with the ECPSSR values and most of other experimental values within the error band of 30%. And the trend of the variation of experimental data is very similar to that of all the compared values. Thus it is concluded that these data can be utilized as the basic data of PIXE analysis for 0.5~1.2-MeV proton beam within the 20% uncertainty.

To improve the present work further, the improvements of the X-ray detection systems, further evaluations for low energy cross-section data, the stabilizations of the accelerator operation, and the increase of the beam energy are required.

References

1. H.J. Woo, "System Calibration of SNU 1.5MV Tandem Van de Graaff and its Utilization for PIXE Analysis", Ph. D. Thesis, Dept. of Nuclear Engineering, Seoul National University (1986).
2. E.C. Montenegro, G.B. Baptista and P.W.E.P. Duarte, *Atomic Data & Nucl. Data Tables*, **22**, 134 (1978).
3. W.H. Tait, "Radiation Detection", Butterworth Inc., London, 386 (1980).
4. J.H. Scofield, *Phys. Rev.*, **A9**, 1041 (1974).
5. J.H. Scofield, *Atomic Data & Nucl. Data Tables*, **14**, 121(1974).
6. B.H. Choi, *Phys. Rev.*, **A4**, 1002 (1971).
7. H. Tawara, K. Ishii, S. Morita, H. Kaji and T. Shiokawa, *Phys. Rev.*, **A11**, 1560 (1975).
8. W. Bambynek, B. Crasemann, R.W. Fink, H.U. Freund, H. Mark, C.D. Swift, R.E. Price and P.V. Rao, *Rev. Mod. Phys.*, **44**, 716 (1972).
9. J.H. Scofield, *Phys. Rev.*, **179**, 9 (1933).
10. O. Benka and A. Kropf, *Atomic Data & Nucl. Data Tables*, **22**, 219 (1978).
11. G. Basbas, W. Brandt and R. Laubert, *Phys. Rev.*, **A7**, 983 (1973).
12. D.D. Cohen and M. Harrigan, *Atomic Data & Nucl. Data Tables*, **33**, 255 (1985).
13. R. Lear and T.J. Gray, *Phys. Rev.*, **A8**, 2469 (1973).

14. E. Laegsgaard, J.U. Andersen and F. Hogedal, *Nucl. Instr. & Meth.*, **169**, 293 (1980).
15. J.S. Lopes, A.P. Jesus and S.C. Ramos, *Nucl. Instr. & Meth.*, **169**, 311 (1980).
16. E. Koltay et al., *Z. Phys.*, **A278**, 299(1976).
17. F. Hopkins, R. Brenn, A.R. Whittemore, J. Karp and S.K. Bhattacherjee, *Phys. Rev.*, **A11** 916(1975).
18. D. Bhattacharya, S.K. Bhattacherjee and S.K. Mitra, *J. Phys.*, **B13**, 967 (1980).
19. C. Bauer, H. Richter, P. Gippner, R. Mann, W. Ruddolph, B. Eckhardt and K.O. Groeneveld, *Z. Phys.*, **A303**, 13 (1981).
20. R.S. Sokhi and D. Crumpton, *Nucl. Instr. & Meth.*, **181**, 5(1981).
21. C.V. Barros Leite, N.V. de Castro Faria and A.G. de Pinho, *Phys. Rev.*, **A15**, 943 (1977).